

Holographic realization of hexagonal two dimensional photonic crystal structures with elliptical geometry

Yung-Jr Hung,^{a)} San-Liang Lee, and Yen-Ting Pan

Department of Electronic Engineering, National Taiwan University of Science and Technology, No. 43, Sec. 4, Keelung Rd., Taipei 106, Taiwan

Brian J. Thibeault and Larry A. Coldren

Department of Electrical and Computer Engineering, University of California at Santa Barbara, Santa Barbara, California 93117

(Received 29 December 2009; accepted 30 August 2010; published 22 September 2010)

A complete investigation of holographic photonic crystal structures has been conducted. From both theoretical and experimental results, profiles of resultant patterns under different process conditions can be estimated and controlled. The use of antireflection layers is crucial for realizing submicron photonic crystals with good uniformity over a large area. We successfully realize submicron-scale photonic crystal templates on silicon substrates with an aspect ratio of 2.5 and good quality by a laser holography technique. The samples are highly uniform in an area of $>2 \times 2 \text{ cm}^2$ and present good reproducibility. A lift-off process is performed to transfer inversed pillar patterns into a chromium hard mask for the following dry etching into silicon substrates. A single-step deep reactive ion etching with controlled mixture of $\text{Ar}/\text{SF}_6/\text{C}_4\text{F}_8$ gases is used to directly transfer pillar patterns into silicon. Transferred patterns with a high aspect ratio and vertical sidewalls (no scalloping) are demonstrated over a large area. © 2010 American Vacuum Society.

[DOI: 10.1116/1.3491185]

I. INTRODUCTION

A photonic crystal (PhC) is an artificial periodic structure that controls the behavior of photons. Since its first introduction by Yablonovitch¹ and John,² PhCs have been used to realize functional devices for optical networking, image display, biomedical sensing, and solar cells for the past decades. However, due to the extreme difficulty to integrate three-dimensional PhCs with other optoelectronic devices, most researchers have been focusing on the two-dimensional (2D) PhC structures. The use of e-beam lithography to realize 2D PhC structures with accurately controlled feature size is a direct and common solution. However, the disadvantages of being time consuming and having low throughput and high cost are serious shortcomings for this technique. Although nanoimprint lithography may be potentially a flexible and high-throughput solution, the key concerns of overlay, defects, and template patterning may affect the resultant pattern and its photonic bandgap (PBG) properties. On the other hand, laser holography lithography based on two-beam interference principle, has been successfully applied over 1 decade to manufacture periodic structures for a wide variety of uses. It is an attractive method for periodic pattern generation over a large area with high throughput and low cost. Although it is much harder to accurately control the location and feature size of submicron-scale periodic structures in this method, photonic crystals with slight structural variations are still suitable for many applications due to its relative wide PBGs.³

Some groups indeed realized 2D periodic pillars or holes by means of laser holography technique.^{4–13} However, most results were fabricated either on a silicon substrate with a larger micron-level periodicity or on a glass substrate with a submicron periodicity. To our knowledge, very few groups have really attained submicron holographic PhCs on a silicon substrate. A factor that may have contributed to this is the serious back-reflection (or so-called standing wave effect) between air and silicon substrates (the refractive index is 5 for 325 nm of incident wavelength), which would otherwise degrade the process latitude. To overcome this bottleneck, a buffer material between air and silicon substrates as an anti-reflection (AR) layer is necessary to relax the back-reflection issue.

In this work, we focus on theoretical and experimental investigation of holographic photonic crystal structures on silicon substrates. Hexagonal 2D photonic crystals with an elliptical geometry are realized by laser holography with a double-exposure and a rotation of sample. An analysis model is developed to calculate the back-reflection and try to minimize it by using an AR coating layer. Thanks to the nonlinear nature of positive photoresist (PR), 2D periodic holes and pillars can be realized by controlling the total exposure energy onto the surface of photoresist. How the profile is affected under different development time is also investigated. After successfully realizing photonic crystal templates, a lift-off process is performed to transfer pillar patterns into a chromium hard mask with inversed structures for the following reactive ion etching (RIE) into silicon substrates. A single-step deep reactive ion etching (DRIE) with controlled

^{a)}Electronic mail; d9502307@mail.ntust.edu.tw

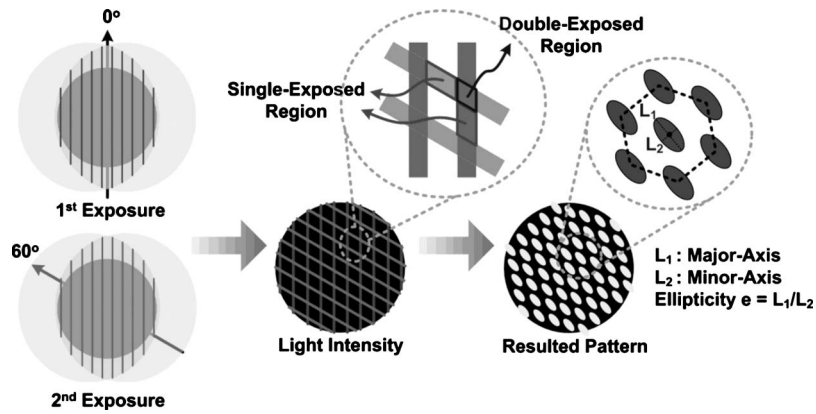


FIG. 1. Schematic diagram of process procedures for realizing hexagonal 2D photonic crystals by means of two-beam interference principle with double-exposure steps.

mixture of Ar/SF₆/C₄F₈ gases is used to directly transfer pillar patterns into silicon with a high aspect ratio and vertical sidewalls (no scalloping).

II. HOLOGRAPHIC CONCEPTS

As with conventional holography, using single-exposure of three-beam interference to obtain a two-dimensional interference pattern was theoretically¹⁴ and experimentally¹³ discussed. However, this method suffers from complicated process setup since the resultant pattern depends on both the propagation and polarization parameters of each beam. A holography setup based on a multiple exposure of two-beam interference principle is attractive due to its simplicity and flexibility.^{4,8} A hexagonal array with a circular shape can be realized by triply exposing the same interference pattern with the sample rotated by 0°, 60° and 120°, respectively.^{8,12} However, this method may suffer from an alignment issue for realizing submicron hexagonal 2D structures over a large area.³ On the contrary, if double exposure of two-beam interference is executed at 0° and 60°, one can fabricate 2D periodic structure with a hexagonal lattice of elliptical geometry.^{3,4,6,8,10,12} Although the shape of resultant pattern is elliptical, there still exists a photonic bandgap in this structure.³ The relatively simple fabrication procedures and experimental setup of this method will improve the manufacturing yield, thus reducing the cost.

Figure 1 shows the schematic diagram of process procedures for realizing hexagonal 2D photonic crystals by means of two-beam interference principle with double-exposure steps. The sample is exposed to a one-dimensional interference stripe with a sinusoidal intensity profile at 0° and 60°. On the resultant 2D intensity distribution, the area covered only by one of exposure steps is referred to single-exposed region while the area overlapped by both exposure steps is the double-exposed region. The nonexposed region refers to the area where almost no exposed energy falls during both exposure steps. With a carefully controlled process, it is possible to realize a hexagonal lattice with an elliptical geometry. The ellipticity (e) of the resultant pattern is defined as the ratio between the length of major-axis (L_1) and minor-axis (L_2) of the ellipse.

III. THEORETICAL MODELING

Before fabricating two-dimensional periodic structures, a simulation model to calculate the profiles of holographically recorded patterns is necessary to initially understand the effects of each process parameter. The profile of recorded structures in photoresist depends on the light exposure pattern, photoresist sensitization and development. In the case of double-exposure in two-beam interference, the light exposure pattern can be described by

$$I_{\phi_1}(x, y) = 2I \cos^2[\text{OPD} \times (x \cos \phi_1 + y \sin \phi_1)],$$

$$I_{\phi_2}(x, y) = 2I \cos^2[\text{OPD} \times (x \cos \phi_2 + y \sin \phi_2)],$$

$$I_{\text{total}}(x, y) = I_{\phi_1}(x, y) + I_{\phi_2}(x, y), \quad (1)$$

where I is the intensity of laser beam; OPD is the optical path difference which is defined by $\text{OPD} = \pi[\sin(\theta_1) + \sin(\theta_2)]/\lambda$, where θ_1 and θ_2 are the incident angle of beam 1 and beam 2, and λ is the incident wavelength; ϕ_1 and ϕ_2 are the rotating angles of sample in the first and second exposure steps. Thus the total exposure pattern can be obtained by adding the intensity distribution $I(\phi_1)$ and $I(\phi_2)$ of the first and second exposure energies. The photosensitization process was mathematically represented by writing the inhibitor concentration m as a function of irradiance.¹⁵

$$m_{xy}(z) = \exp[-CI(x, y)\Delta T], \quad (2)$$

where C is the kinetic exposure rate constant and ΔT is the exposure time. In this article, we use normalized exposure energy $CI(x, y)\Delta T$ for obtaining the inhibitor concentration which ranges from 0 (complete exposed) to 1 (unexposed). The dissolution rate V of the photoresist in a developer can be described as¹⁶

$$V_{xy}(z) = V_{\text{max}} \frac{(a+1)[1-m_{xy}(z)]^n}{a+[1-m_{xy}(z)]^n} + V_{\text{min}}, \quad a = \frac{n+1}{n-1} (1 - m_{\text{th}})^n, \quad (3)$$

where V_{max} and V_{min} are the dissolution rates of the fully exposed and nonexposed photoresists, respectively (they are determined by the concentration of developer); a is a function of the inhibitor concentration threshold m_{th} at the onset

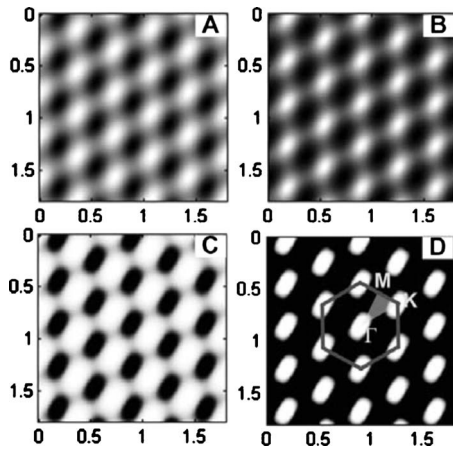


FIG. 2. (a) Light intensity distribution under double-exposure of two-beam interference. (b) Inhibitor concentration in the exposed photoresist during the photosensitization process. (c) Dissolution rate of the exposed photoresist in a developer. (d) Resultant patterns after development. Two-dimensional periodic patterns with a hexagonal lattice of elliptical pillars can be realized.

of dissolution, and n is the number of molecules of the product of the photoreaction that reacts with the developer to dissolve a resin molecule. Therefore, the remaining photoresist thickness $z(x, y, t)$ can be obtained by a simple integration of the dissolution rate $V(x, y, z)$.

$$z(x, y, t) = z(x, y, t_0) - \int_0^t V(x, y, z) dt. \quad (4)$$

Figure 2 shows the step-by-step transition process for the generation of two-dimensional hexagonal pillars. Parameters used in this model are shown in Table I. Due to the double-exposure process, there exist three different intensity levels (double-exposed region, single-exposed region, and non-exposed region) in the light intensity distribution which may result in three different exposure energies. Thanks to the nonlinear nature of the photoresist,¹⁷ we can slightly overexpose to let the double- and single-exposed regions have almost the same cross-link effect to eliminate this problem. With optimal process condition, a well-defined arrayed pattern can be holographically realized.

Although the exposure pattern is sinusoidal, we can still produce a photoresist pattern with a squarelike profile by

developing in strong nonlinear conditions. On the other hand, a sinusoidal profile will be expected if the development is in linear conditions because the isotropy of wet development produces a narrowing on the top of the structures.¹⁶ That is, for the case of low exposure energy and high concentration developer, we cannot obtain isolated patterns since the dissolution rate in single- and double-exposed regions is still low and the resultant profile under high concentration developer (or long development time) becomes sinusoidal. However, if high exposure energy and low concentration developer (or short development time) is used for the same purpose, isolated patterns with vertical sidewalls become possible due to the sufficient dissolution rate in both single- and double-exposed regions such that the isotropic wet etching effect is eliminated.

Periodic pillars can be realized holographically by using a positive photoresist,⁵⁻⁷ while arrayed holes can be fabricated by using a negative photoresist.^{8,9,11,12} However, the use of negative photoresist suffers from fabrication problems including the resolution limit and the fact that it is harder to be removed by wet etching. On the other hand, if we utilize the nonlinearity nature of positive photoresist, we can obtain periodic holes by carefully controlling the exposure doses to have above-threshold dissolution rate in the double-exposed region and below-threshold dissolution rate in the single- and nonexposed regions. After development, only the photoresist in the double-exposed region can be removed and two-dimensional periodic holes can be realized. If the total exposure energy is enough to have above-threshold dissolution rate in both double- and single-exposed regions, two-dimensional periodic pillars will be realized. Figure 3 shows the evolution of the calculated profiles as the normalized exposure energy increases. When the normalized exposure energy is below 0.8 (above 1.2), the resultant pattern is a periodic hole (pillar) structure. The transitioned structure is observed when the exposure energy is between 0.8 and 1.2. From the calculated profile under 0.6 normalized exposure energy, we can find that the photoresist in the double-exposed region is totally removed, while that in the single-exposed region is almost remained, forming perfect hole patterns. There is a maximum thickness of photoresist for fabricating perfect holes or pillars with controlled exposure dose onto the photoresist.

TABLE I. Parameters for simulation of profiles of holographic photonic crystals.

Parameter	Symbol (unit)	Value
Incident wavelength	λ (nm)	325
Incident angle	θ_1, θ_2 (deg)	30, 30
Rotating angle of sample	ϕ_1, ϕ_2 (deg)	0, 60
Normalized exposure energy	$CI(x, y)\Delta T$ (a.u.)	variable
Number of molecules of the product of the photoreaction	n	6
Dissolution rate of the nonexposed and full-exposed photoresist	V_{\min}, V_{\max} (nm/s)	0.15, 54
Inhibitor concentration threshold at the onset of dissolution	m_{th}	0.61
Thickness of photoresist	T (nm)	200
Development time	DT (s)	Variable

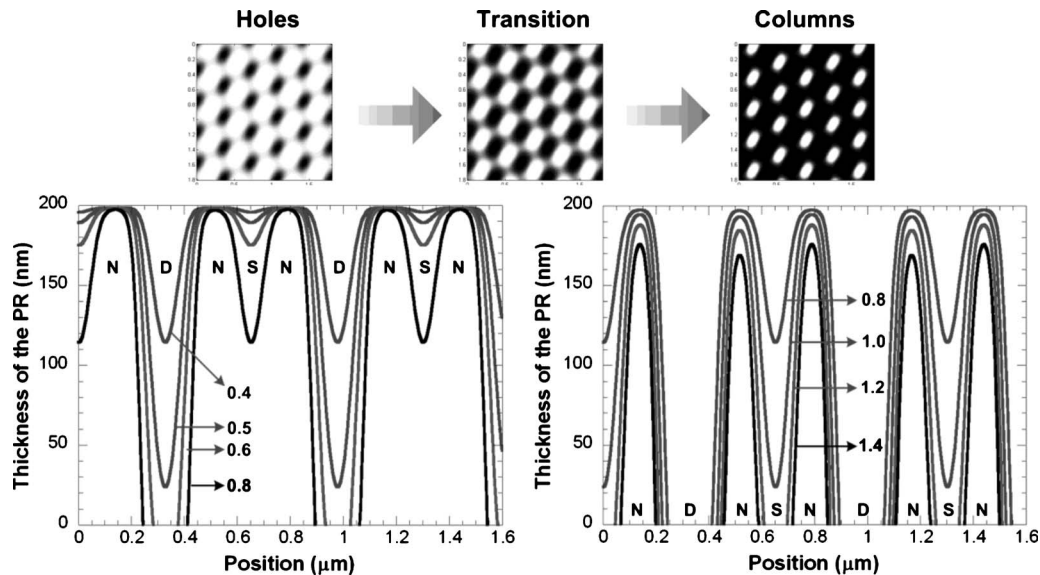


FIG. 3. Evolution of the calculated profiles with the normalized exposure energy (the numbers in the figure) for positive photoresist films double exposed to an interference pattern. By carefully controlling the total exposure doses, two-dimensional periodic holes or pillars can be realized by using a positive photoresist. Development time in this figure is set to 8 s (N: nonexposed region, S: single-exposed region, and D: double-exposed region).

Figure 4 shows the calculated profiles under different exposure doses. Periodicity of the hexagonal patterns in this calculation is set to 420 nm. Hollow-square and solid-circle symbols in Fig. 4 show the diameters of holes and pillars, respectively, while the hollow-circle and solid-diamond symbols show the ellipticity of holes and pillars, respectively. An increased (decreased) diameter of holes (pillars) for both major and minor axes of elliptical structure is expected as the exposure energy increases. From the overlap point of diameter curves, we know the maximal air fill factor (the ratio between the averaged radius of ellipse and the periodicity of resultant pattern) of holographic patterns is about 40% for both holes and pillars. The calculated ellipticity of the resultant patterns is about 1.73 throughout all exposure conditions. How the profile of the resultant patterns is affected under

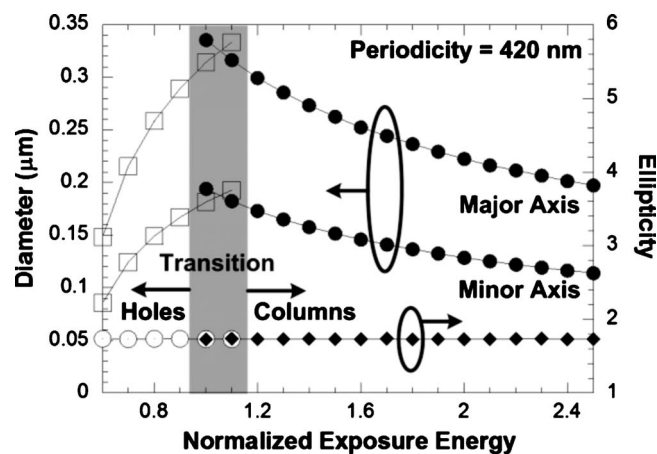


FIG. 4. Calculated profiles under different exposure energies. (Hollow-square and solid-circle symbols show the diameters of holes and pillars, respectively, while hollow-circle and solid-diamond symbols show the ellipticity of holes and pillars, respectively.)

different development time is also investigated theoretically. Once the exposure energy is determined, sufficient development time is necessary to completely generate patterns. The aspect ratio of the resultant pattern will increase as the development time increases. The width of the pillars will be reduced as the aspect ratio reaches its maximum value. With neglectable back-reflection issue, there is only about 2 nm reduction rate for overdeveloped process.

Photonic bandgap maps of the calculated profiles under different exposure energies are shown in Fig. 5. Due to the noncircular geometries of the resultant patterns, the addition of new directions to represent one-quarter of the Brillouin zone is necessary.⁶ Detailed discussion can be found in previous works.^{3,6} As we expected, there exist TM-mode (electric field in plane) gaps in hole arrays, while TE-mode (mag-

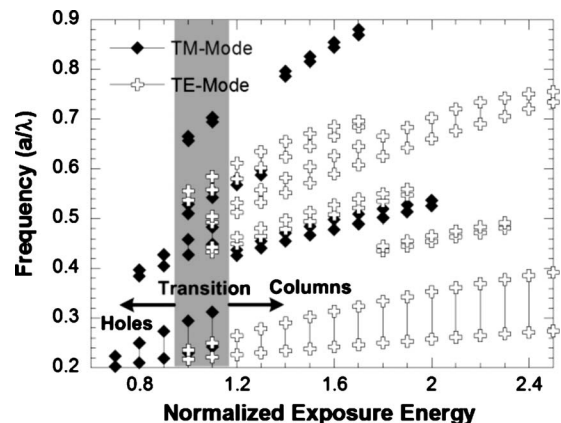


FIG. 5. Photonic bandgap maps of the calculated profiles under different exposure energy. (Solid-diamond and hollow-cross symbols show the TM- and TE-mode gaps, respectively.)

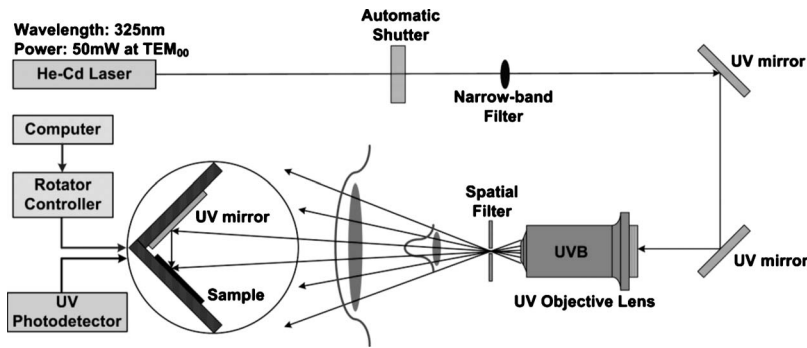


FIG. 6. Schematic diagram of our laser holography system

netic field in plane) gaps dominate pillar arrays. The gap size is affected according to the geometry of resultant patterns depending on the exposure energy.

IV. EXPERIMENTAL DEMONSTRATION

Figure 6 shows the schematic diagram of our holographic setup which consists of a light source, a narrow-band filter, an UV objective lens, a spatial filter, and a sample stage. The light source is a 50 mW He–Cd laser emitting at a wavelength of 325 nm in a single transverse mode. A 325 nm laser-line filter with 1.2 nm bandwidth and $>80\%$ transmission is used to guarantee the pure light from the He–Cd laser. An UV objective lens and a spatial filter are used to enlarge the total area of the light field at the sample stage and to block the noise from the laser source. At the sample stage, an UV-mirror and a sample holder plate are fastened together at 90° . All of the components in this holography system are transparent at 325 nm. By simply adjusting the stage orientation with respect to the direction of the laser beam, the periodicity of the resultant patterns can be easily controlled.

A. Realization of PhC templates with the help of AR coating

Due to the presence of an additional interference fringe parallel to the surface of sample, called standing waves, the use of high refractive-index substrates generate serious back-reflection problems to the lithography. This problem may be even stronger if the applied photoresist film is thicker than one-half period of the standing wave pattern. To reduce the contrast of the standing wave, some materials with the right thickness are proposed as AR coating layers.¹⁸ The use of dielectric materials such as silicon dioxide or silicon nitride with an accurate thickness can also be served as the buffer layer to eliminate the back-reflection problem. However, reflectivity variation due to imperfect AR layers is an uncertain factor in the process. Commercial bottom AR coating materials are available from photoresist manufacturers. Such coatings provide a gradual variation of refractive index between the photoresist and substrate to reduce the back-reflection from the interface as well as to absorb the transmitted light, leading to wider thickness tolerance for the AR coating layers.

To calculate the back-reflection into the resist layer, we developed an analytical model by using a transfer matrix and

modified transmission and reflection coefficients,¹⁹ given the real and imaginary parts of the index of refraction for the materials and the incident angle θ of the two laser beams. Figure 7(a) shows the reflectivity variation under different thicknesses of AR coating layers with an incident wavelength of 325 nm. The structure of the test sample is also shown in the inset of Fig. 7(a). Back-reflection of the real photoresist/ARC/silicon sample with an incident angle of 30° is also calculated. Thickness and refractive index of the AR coating and photoresist layer are characterized by an ellipsometer (Rudolph AutoEL-III) and thin-film measurement system (Filmetrics F20-UV).

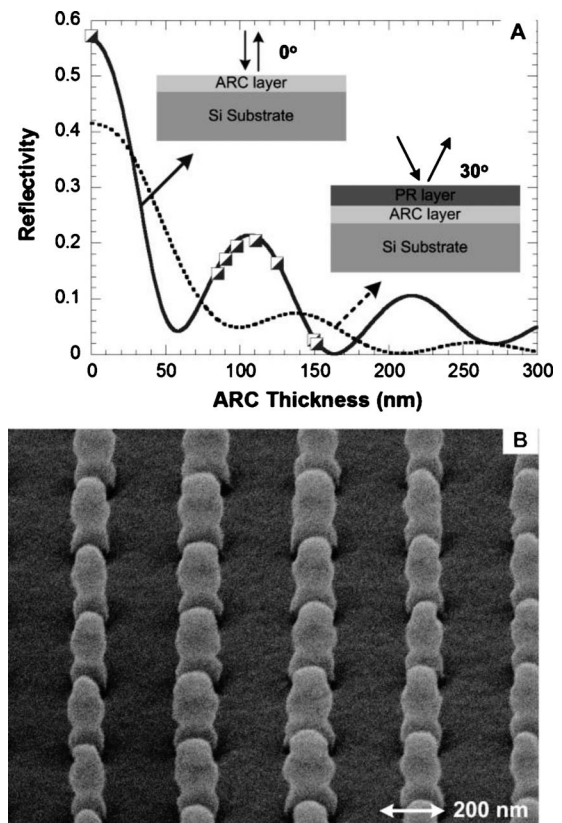


FIG. 7. (a) Reflectivity variation under different thickness of AR coating layer with an incident wavelength of 325 nm. The structure of the test sample is shown in the inset of the figure. (Solid and dot curves are simulation results while square symbols are experimental data). (b) 200 nm thick PhC templates using an 80 nm thick AR coating layer. Sidewall distortion on the resultant patterns caused from back-reflection can be clearly seen.

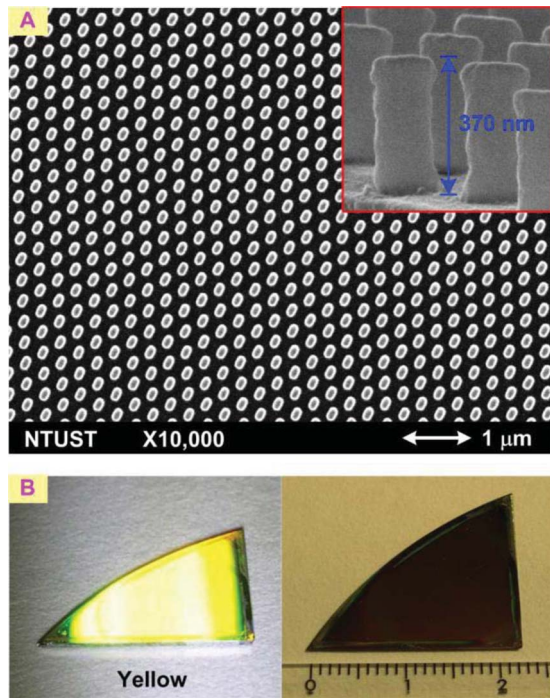


FIG. 8. (Color online) (a) SEM pictures of fabricated two-dimensional hexagonal pillars. 370 nm thick PhC templates with a high aspect ratio and vertical sidewalls are realized using a 160 nm thick AR coating layer. (b) Photographs of the resultant samples under tilted angles of illumination. Bright and uniform diffracted light throughout the sample proves a good quality of the resultant patterns. The samples are highly uniform in an area of $>2 \times 2$ cm² and present good reproducibility.

Without the help of AR coating, it is difficult to fabricate submicron patterns on silicon substrates due to serious back-reflection problem. Although photoresist with a thickness of half standing wave period can be used to avoid pattern distortion or collapse, only ~ 50 nm thick PhC templates is not sufficient as a mask for pattern transferring. 200 nm thick patterns can be realized using an 80 nm thick AR coating layer between photoresist and silicon substrate, as shown in Fig. 7(b). However, we can clearly see the distortion on the sidewalls of resultant patterns due to insufficient reduction of back-reflection.

370 nm thick PhC templates with an aspect ratio of 2.5 and vertical sidewalls are demonstrated with the help of a 160 nm thick AR coating layer, as shown in Fig. 8(a). Fabrication flow for this well-defined template is investigated as follows. Silicon substrate is cleaned by ultrasonification in acetone and isopropanol and blown dry with nitrogen gas. A 160 nm AR coating layer (Brewer Science XHRiC-11 ARC) is deposited by spin coating with a solution at 1500 rpm for 70 s. After prebaking the AR coating layer on a hot plate at 165° for 60 s, a 370 nm positive photoresist layer (OHKA THMR-M100) is deposited at 2000 rpm for 30 s and soft baked again at 90° for 90 s. The sample is then transferred to the laser holography system and exposed twice with a dose of 30.24 mJ/cm² for each exposure. Following the double-exposure, a postexposure bake (PEB) is performed on a hot plate at 115° for 120 s to further reduce the standing-wave

effect. After that, the sample is dipped into standard 2.38% TMAH photoresist developer (AZ-300MIF) for 10 s to attain a periodic structure. After development, the sample is rinsed in de-ionized water and finally hard baked at 100° for 60 s to complete the cross-linking process. Figure 8 shows the SEM pictures and photographs of the resultant 2D hexagonal pillars. By using a flashlight to illuminate the PhC sample with a tilted angle in the directions perpendicular to double-exposure directions, a bright diffracted light throughout the sample and a change in color under different angles of illumination is observed, as shown in Fig. 8(b), indicating that the resultant PhC structure is well orientated throughout the sample with high uniformity and superior quality. The samples are highly uniform in an area of $>2 \times 2$ cm² and present good reproducibility.

B. Resultant profiles under different process conditions

In order to investigate the resultant profiles under different exposure energy, eight 200 nm thick hexagonal photonic crystal samples are fabricated with a development time of 5 s and exposure times of 100, 110, 120, 130, 150, 170, 190, and 210 s for each exposure, corresponding to the exposure doses of 14.4 mJ/cm² (sample A), 15.84 mJ/cm² (sample B), 17.28 mJ/cm² (sample C), 18.72 mJ/cm² (sample D), 21.6 mJ/cm² (sample E), 24.48 mJ/cm² (sample F), 27.36 mJ/cm² (sample G), and 30.24 mJ/cm² (sample H). Other process conditions such as PEB are the same as described in Sec. IV A except the rotational speed for the spin-on photoresist (5000 rpm for 30 s). Figure 9 shows the experimental profiles under different exposure doses. SEM pictures of the corresponding structures are shown around the analytical plot, which shows the diameter and ellipticity of the resultant patterns with the exposure energy.

We can find that air-hole patterns (samples A–C) can be realized with lower exposure energy while periodic pillars (samples E–H) can be realized with higher exposure energy. As the exposure energy increases, the diameters of holes increase for both axes of elliptical structure. An increase of the ellipticity of holes is observed. This may be mainly due to the slightly difference of exposure energy between the first and second exposure steps. The difference of exposure energy between the two exposure steps is due to nonuniform exposure and the rotation of sample. For pillar patterns, the diameters decrease for both axes of the ellipse as the exposure energy increases. The ellipticity of the pillars is always around 1.47 for different exposure energies. The reason for the ellipticity difference between experimental (Fig. 9) and theoretical (Fig. 4) results may be due to the other process effects such as PEB, which was not considered in our simulation model.

The effect of development time for the resultant profiles is also investigated here. Four 200 nm thick hexagonal photonic crystal samples are fabricated with an exposure energy of 21.6 mJ/cm² and development times of 5 s (sample A), 10 s (sample B), 15 s (sample C), and 20 s (sample D). Figure 10 shows the experimental profiles under different development

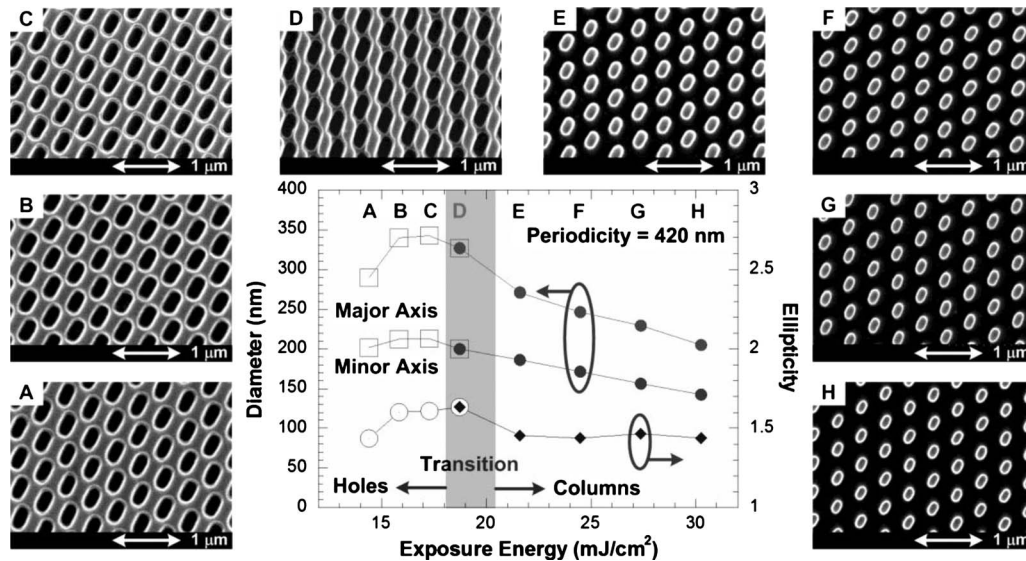


FIG. 9. Experimental profiles under different exposure energy. Eight uniformly hexagonal photonic crystal samples are fabricated with a lattice constant of 420 nm. SEM pictures of the corresponding structures are shown around the analytical plot which shows the diameter and ellipticity of the resultant pattern with the exposure energy. (Hollow-square and solid-circle symbols show the diameters of holes and pillars, respectively, while hollow-circle and solid-diamond symbols show the ellipticity of holes and pillars, respectively.)

time. SEM pictures of the corresponding structures are shown above the analytical plot, which shows the diameter and ellipticity of the resultant pattern with the development time. The width of the pillars is reduced as the development time increases. The reduction rates for the major and minor axes of ellipse are about 2.8 and 1.7 nm/s, which agree with our theoretical results. The difference of reduction rate between two axes of ellipse may be also due to the slightly difference of exposure energy between the first and second exposure steps. Such low reduction rate for overdeveloped process is also due to the help of good AR coating. From

Figs. 9 and 10, we can find that the fabrication tolerance for holographic realizing 2D photonic crystals by double exposure process is very wide in terms of exposure energy and development time. The total exposure energy will determine the geometry of resultant patterns. Development time will not affect the patterns a lot.

C. Pattern transfer into silicon

Polymeric periodic arrays may seem unlikely to yield useful photonic structures since the refractive index of such ma-

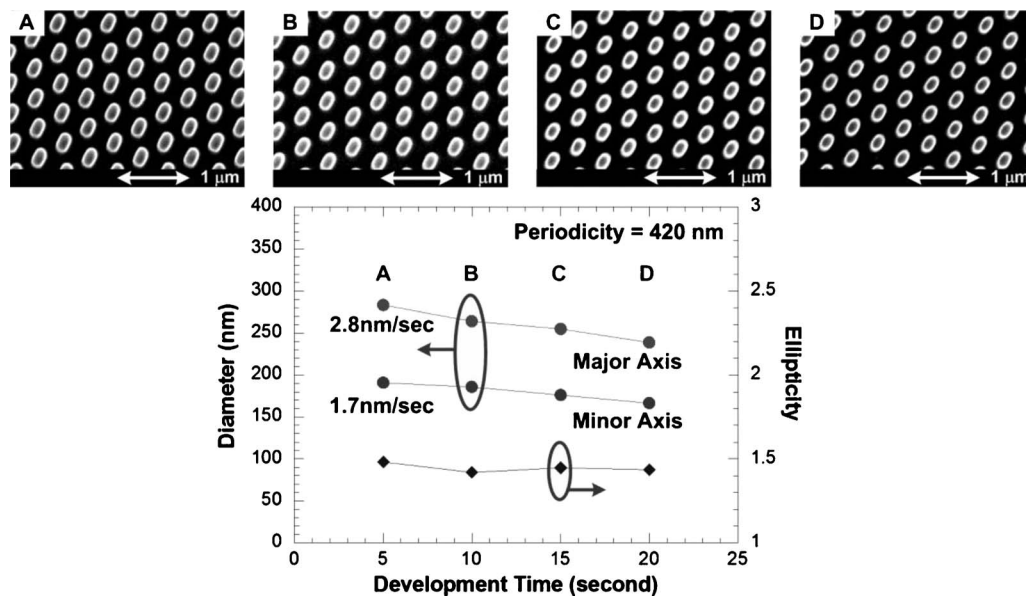


FIG. 10. Experimental profiles under different development time. Four 200 nm thick hexagonal photonic crystal samples are fabricated with a lattice constant of 420 nm. SEM pictures of the corresponding structures are shown above the analytical plot which shows the diameter and ellipticity of the resultant pattern with the development time. (Solid-circle symbol shows the diameter of pillars while solid-diamond symbol shows the ellipticity of the pillars.)

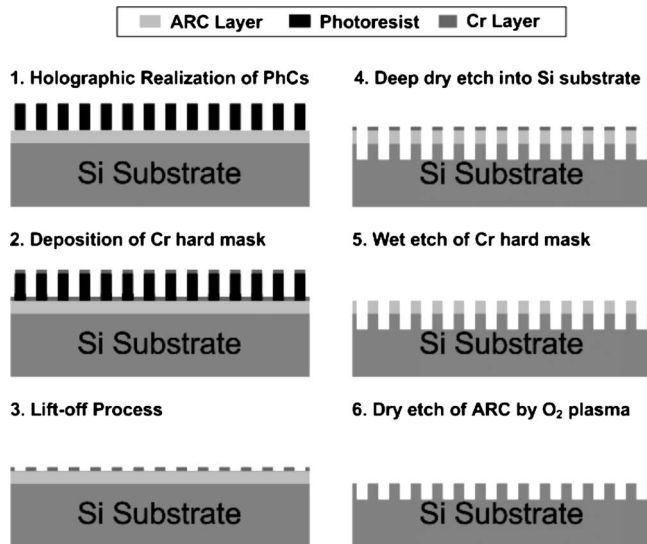


FIG. 11. Sequence of the experimental steps for transferring PhC patterns into silicon substrate by means of lift-off process and etching technique.

materials are substantially less than those of the more traditionally used solid-state materials such as silicon. Thus they are usually used as intermediate templates to create photonic lattices with higher index materials. To deep transfer the patterns into silicon substrate, a hard mask such as chromium (Cr) is often used to provide high etching selectivity for the following deep etching process but metal hard mask patterning can be difficult. It is also possible to transfer patterns into metal layer by wet etching process. However, undercutting due to isotropic etching makes wet etching useless for nanometer-scale patterns. Another way to transfer the patterns is to perform a lift-off process but the resultant patterns will be inverted.

We perform a lift-off process to transfer patterns into a chromium hard mask layer for the following dry etching into silicon substrate. The fabrication flow of pattern transfer is shown in Fig. 11. SEM pictures of the resultant patterns after Cr evaporation (procedure 2 of Fig. 11), lift-off using a blue-tape (procedure 3 of Fig. 11), and dry etching into silicon (procedure 6 of Fig. 11) are shown in Fig. 12. After preparing a 370 nm thick hexagonal PhC template with a lattice constant of 375 nm by means of laser holography method, as described in Sec. IV A, a 35 nm chromium film is deposited

onto the photoresist template by angled e-beam evaporation to generate a hard mask layer, as shown in Fig. 12(a). Since the resultant patterns are not clean by conventional lift-off method using an acetone solution (removed Cr patterns are usually stuck back onto the samples), the following lift-off process is carried out by using a blue tape to stick the photoresist patterns away from the samples. Although some photoresist patterns are left on the samples after lift-off, they can be easily removed by wet etching or O_2 plasma since no Cr mask lies on the top of photoresist. The resulting patterns are much clean and uniform by this method as shown in Fig. 12(b). Dry etching the patterns into the AR coating layer and silicon substrate is then carried out using a conventional RIE machine with a CF_4 flow of 5 SCCM (SCCM denotes cubic centimeter per minute at STP), 100W rf power, and a pressure of 80 mTorr. After performing 15 min of dry etching procedure, the photonic crystal pattern is then transferred through the 160 nm AR coating layer and into the silicon substrate to a maximum depth of about 650 nm. Since there is still Cr on the surface, deeper etching is possible. To remove the remaining Cr and AR coating layers on the surface of the sample, a wet etching process is used to remove the Cr layer, while oxygen plasma is then used to clean the residual AR coating layers. Figure 12(c) shows the side-view of the transferred silicon PhC structures. Highly uniform photonic crystals on silicon substrates with a high aspect ratio (>4) and vertical sidewalls are demonstrated over a large area.

Contrary to conventional schemes for PhC pattern transfer, a novel DRIE is developed and utilized for etching PhC pillar patterns into silicon substrates. DRIE is mainly used for microelectromechanical systems and microfluidic device fabrication. Multiple cycles of the two-step Bosch process enable anisotropic etching of silicon with high mask selectivity ($>200:1$ for silicon oxide and $>75:1$ for PR) and high etching rate (several $\mu\text{m}/\text{min}$). However, this technique is not suitable for etching nanostructures due to its scalloping of the sidewalls (the peak-to-valley height is typically the scale of around several hundred nanometers). Recently, with the development of this technology, Choi *et al.*²⁰ directly transferred 20 nm thick photoresist patterns into silicon with controlled sidewall profiles using a Bosch process. More recently, Morton *et al.*²¹ realized silicon pillar array with an aspect ratio of $>50:1$ and a peak-to-valley height (scalloping) of ~ 10 nm using a Bosch process with an optimized

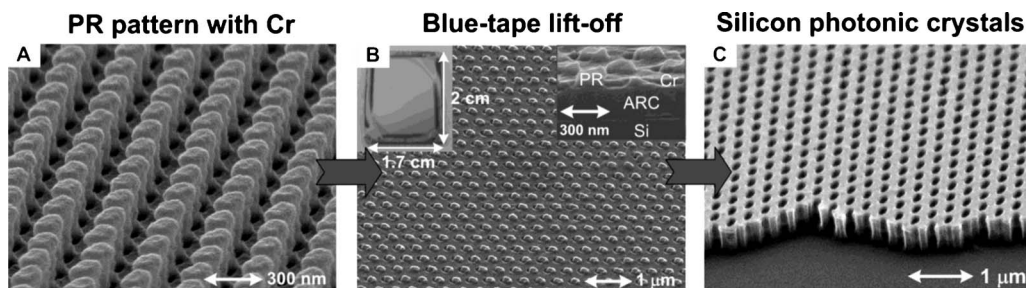


FIG. 12. SEM pictures of the resultant patterns after (a) Cr evaporation (procedure 2 of Fig. 11), (b) lift-off using a blue-tape (procedure 3 of Fig. 11), and (c) dry etching into silicon (procedure 6 of Fig. 11)

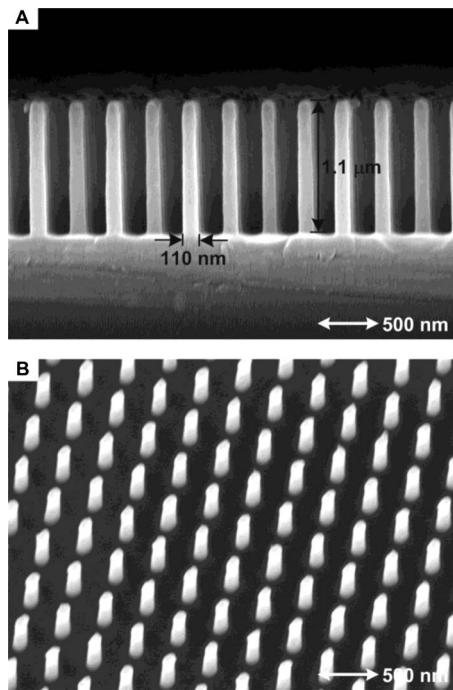


FIG. 13. Cross-sectional and tilted SEM views of vertical silicon nanopillars with an aspect ratio of 10 using a single-step deep reactive ion etching and controlled mixture of Ar/SF₆/C₄F₈ gases.

etching conditions. However, the scalloping of the sidewalls cannot be avoided due to the cyclic deposition/etching nature of the Bosch process, resulting in periodic ripples on the sidewalls. We have developed a means of directly transferring photoresist patterns into silicon using a single-step DRIE and controlled mixture of Ar/SF₆/C₄F₈ gases. With an optimized gas mixture for balancing the deposition (C₄F₈ flow) and etching rate (SF₆ flow), pillars with vertical sidewalls can be realized. During the etching process, the scalloping of the sidewalls can be avoided while reserving the high mask selectivity (~85:1) and relatively high etching rate (222 nm/min). Figure 13 shows the cross-sectional and tilted SEM views of the transferred patterns. Silicon nanopillar arrays with an aspect ratio of 10 and vertical sidewalls are achieved with high uniformity over a large area. Systematic analysis of this novel DRIE process is under development and will be discussed in elsewhere.

V. CONCLUSION

A complete investigation of holographic photonic crystal structures has been conducted. Hexagonal photonic crystals with an elliptical geometry can be realized by performing a double-exposure of laser holography method. Theoretical and experimental results show that two-dimensional periodic holes or pillars can be realized depending on the total exposure energy onto the surface of positive photoresist layer. The photonic band diagrams for the PhC structures under different exposure doses are also analyzed. Width reduction of the resultant patterns under different development time is

also investigated. An analysis model is developed and an antireflection layer is used for eliminating the back-reflection from the substrate. Optimized process procedures for holographically realizing photonic crystals on a silicon substrate with good quality are addressed. Submicron photonic crystal templates with an aspect ratio of 2.5 and vertical sidewalls are demonstrated. The samples are highly uniform in an area of $>2 \times 2$ cm² and present good reproducibility.

A lift-off process is performed to transfer inversed pillar patterns into a chromium hard mask for the following deep dry etching into silicon substrates using a conventional RIE machine. A single-step DRIE with controlled mixture of Ar/SF₆/C₄F₈ gases is used to directly transfer pillar patterns into silicon. Transferred patterns with a high aspect ratio and vertical sidewalls are demonstrated by those methods over a large area. We believe that holographic photonic crystals will be a low-cost choice for a variety of industry applications, including efficiency enhancement of light emitting diodes and solar cells, biomedical sensing, and photonic integrated circuits.

ACKNOWLEDGMENTS

The authors would like to thank Chuli Chao of ITRI for his technical assistance. This work was supported in part by the National Science Council, Taiwan, under Grant Nos. NSC95-2219-E-011-004 and NSC97-2219-E-011-009 and by the Ministry of Education under the Top University Program.

- ¹E. Yablonovitch, Phys. Rev. Lett. **58**, 2059 (1987).
- ²S. John, Phys. Rev. Lett. **58**, 2486 (1987).
- ³Y.-J. Hung, S.-L. Lee, and Y.-T. Pan, J. Opt. **12**, 015102 (2010).
- ⁴S. C. Kitson, W. L. Barnes, and J. R. Sambles, IEEE Photonics Technol. Lett. **8**, 1662 (1996).
- ⁵J.-M. Lee, S. H. Oh, C.-W. Lee, H. Ko, S. Park, K. S. Kim, and M.-H. Park, Thin Solid Films **475**, 189 (2005).
- ⁶F. Quiñónez, J. W. Menezes, L. Cescato, V. F. Rodriguez-Esquerre, H. Hernandez-Figueroa, and R. D. Mansano, Opt. Express **14**, 4873 (2006).
- ⁷E. J. Carvalho, M. A. R. Alves, E. S. Braga, and L. Cescato, Microelectron. J. **37**, 1265 (2006).
- ⁸N.-D. Lai, W.-P. Liang, J.-H. Lin, C.-C. Hsu, and C.-H. Lin, Opt. Express **13**, 9605 (2005).
- ⁹L. Pang, W. Nakagawa, and Y. Fainman, Appl. Opt. **42**, 5450 (2003).
- ¹⁰L. Vogelaar, W. Nijdam, H. A. G. M. van Wolferen, R. M. de Ridder, F. B. Segerink, E. Flück, L. Kuipers, and N. F. van Hulst, Adv. Mater. **13**, 1551 (2001).
- ¹¹H. Misawa, T. Kondo, S. Juodkazis, and V. Mizeikis, Opt. Express **14**, 7943 (2006).
- ¹²N. D. Lai, W. Liang, J. Lin, and C. Hsu, Opt. Express **13**, 5331 (2005).
- ¹³I. B. Divliansky, A. Shishido, I.-C. Khoo, T. S. Mayer, D. Pena, S. Nishimura, C. D. Keating, and T. E. Mallouk, Appl. Phys. Lett. **79**, 3392 (2001).
- ¹⁴M. J. Escuti and G. P. Crawford, Opt. Eng. (Bellingham) **43**, 1973 (2004).
- ¹⁵C. A. Mack, J. Electrochem. Soc. **134**, 148 (1987).
- ¹⁶B. A. Mello, I. F. da Costa, C. R. A. Lima, and L. Cescato, Appl. Opt. **34**, 597 (1995).
- ¹⁷A. S. Kewitsch and A. Yariv, Appl. Phys. Lett. **68**, 455 (1996).
- ¹⁸H. L. Chen, T. C. Chu, M. Y. Li, F. H. Ko, H. C. Cheng, and T. Y. Huang, J. Vac. Sci. Technol. B **19**, 2381 (2001).
- ¹⁹R. R. Dammel and R. A. Norwood, Proc. SPIE **2724**, 754 (1996).
- ²⁰C.-H. Choi and C.-J. Kim, Nanotechnology **17**, 5326 (2006).
- ²¹K. J. Morton, G. Nieberg, S. Bai, and S. Y. Chou, Nanotechnology **19**, 345301 (2008).